Int. J. Solids Structures Vol. 30, No. 14, pp. 1891–1906, 1993
Printed in Great Britain

0020–7683/93 $6.00+ .00

SHEAR AND TORSIONAL IMPACT OF CRACKED VISCOELASTIC BODIES—A NUMERICAL INTEGRAL EQUATION/TRANSFORM APPROACH

H. G. GEORGIADIS
Mechanics Division, Box 422, School of Technology, The Aristotle University of Thessaloniki, 54006 Thessaloniki, Greece

(*Received* 27 *July* 1992; *in revised form* 22 *January* 1993)

Abstract—The transient elastodynamic stress intensity factor was determined for a cracked linearly viscoelastic body under impact loading. Two separate geometries along with associated loading conditions were considered. In the first case, the body is in the form of an infinite strip containing a central finite-length crack and is subjected to anti-plane shear tractions. Various strip heights are considered including the possibility of a body of nearly infinite extent. In the second case, the body is of infinite extent containing a finite-length penny-shaped crack and is subjected to radial shear and torsional (twisting) tractions. The analytical parts of the solutions are either given by a previous analysis of H. G. Georgiadis or are obtained from results by G. C. Sih through the use of the correspondence principle. The numerical procedure consists of solving integral equations and then inverting the Laplace transformed solution by the Dubner–Abate–Crump technique. Numerical results were given for the standard linear solid by considering several combinations of material constants.

INTRODUCTION

In the context of Elastodynamic Fracture Mechanics, the main emphasis is placed on determining the stress intensity factor (SIF) as a function of time and of geometrical and material parameters. An important class of problems concerns the *diffraction* of elastic waves by a *pre-existing* crack in the material. The practical need for performing such an analysis, within the scope of Fracture Mechanics, is briefly the following. We assume that a small flaw (in the form of a sharp crack) existing in the particular load-carrying member has escaped the non-destructive testing and we have thus to evaluate the SIF for a critical size of the crack in order to check whether the fracture toughness of the material is exceeded or not. In particular for stress wave loadings, dynamic overshoots of SIF are possible [see e.g. Achenbach (1971), Achenbach and Brock (1973), Brock (1975), Datta (1979) and Karim and Kundu (1988)] and it is interesting to estimate these effects by an exact analysis.

The specific problems considered in the present study concern *viscoelastic* solids and are: (a) the anti-plane shear impact of a strip-like body containing a central finite-length crack, (b) the radial-shear impact of an infinite-extent body containing a penny-shaped crack, and (c) the torsional (twisting) impact of an infinite-extent body containing a penny-shaped crack. The solution to all problems was obtained by a numerical procedure treating initially second-kind Fredholm integral equations and then inverting the Laplace transformed intensity function through the Dubner–Abate–Crump (DAC) technique (Dubner and Abate, 1968; Crump, 1976).

One of the goals of the paper is to emphasize the suitability of the DAC technique for transient elastodynamic mixed BVPs. In fact, we propose the replacement of the inconvenient Orthogonal Polynomials method by the DAC method for reasons explained below. Indeed, the most widely utilized Laplace-transform inversion method in mixed BVPs in elastodynamics is the Orthogonal Polynomials method. This was introduced by Papoulis (1957) and modified by Miller and Guy (1966), and Bellman *et al.* (1966). The research group of G. C. Sih has made an extensive use of the Miller/Guy technique for crack problems (Sih and Chen, 1977, 1981).

However, the Orthogonal Polynomials technique suffers from serious drawbacks. First, there is a "non-uniqueness" in the results since these are strongly dependent upon the choice of the parameters β and δ [in the notation of Miller and Guy (1966)]. Thus, in order to

adjust these parameters, independent analytical results should be available [e.g. already known static results can be used for large times and some classical solutions by Baker (1962), Kostrov (1966), and Thau and Lu (1971) for small time]. Evidently, Sih and co-workers made a very careful and successful application of this technique by comparing their numerical results with available analytical ones over some common time-domains and thus adjusting the parameters β and δ. However, in more advanced fracture mechanics problems, such as viscoelastic or composite-bodies situations, analytical results are not usually available. So, the latter procedure does not work and we need a more reliable inversion method.

Second, by increasing the number of terms N in a certain series expansion, a matrix becomes more and more ill-conditioned leading to instability. Thus, one gets inaccuracy by using few terms and instability by using a lot of terms. Third, a slight error in the values of the transformed function has a great effect on the values of the original function [see for a relative investigation in Cost (1964)]. The latter fact is of considerable importance for mixed boundary value problems in elastodynamics since their Laplace-transformed solution cannot usually be obtained in *closed* form but it is given numerically, following the *approximate* solution of a Fredholm integral equation. Thus, a small error, say 0.1%, in the values of the transformed function alters significantly the form of the original function obtained by orthogonal-polynomial techniques. These three drawbacks may produce questionable results when *independent* results are not available for comparison. Lastly, the overall accuracy of these techniques was found to be very poor in review studies by Davies and Martin (1979), and Narayanan and Beskos (1982).

In the latter survey papers over 20 methods for Laplace-transform inversion were tested and compared. One of the best techniques was found to be the DAC technique. We have adopted this method here and we recommend its further use for mixed BVPs in elastodynamics.

Let us now briefly review work related to the present one. Although many papers have appeared on the *inertial* crack-propagation problem in viscoelastic solids [see e.g. Willis (1967), Atkinson and List (1972), Atkinson and Popelar (1979) and Popelar and Kanninen (1980)], very limited work has been done on the problem of inertial (dynamic) loading of viscoelastic solids containing *stationary* cracks (Georgiadis, 1991 ; Georgiadis *et al.*, 1991). In the latter papers, the problem of plane impact of a cracked viscoelastic body was treated. On the other hand, as regards *purely elastic* response, scattering of waves by penny-shaped cracks has been considered by Mal (1970), Sih and Chen (1977), Krenk and Schmidt (1982), Martin and Wickham (1983), and Keogh (1986), among others.

In the present work, numerical results were obtained for the case of the standard linear solid. The numerical study revealed some interesting features of the problem. For instance, several combinations of material constants may have as a result dynamic SIF overshoots and this fact suggests the necessity of an analysis similar to the present one for other viscoelastodynamic crack problems too.

BASIC RELATIONS AND BOUNDARY CONDITIONS

We consider a general linearly viscoelastic solid under three different geometry and loading conditions, i.e. *anti-plane shear*, *radial shear* and *torsional* deformation. The body is of the form of a long cylinder along the z-axis, having as a cross-section the (x, y) plane. The governing equations are as follows (Fung, 1965; Christensen, 1971).

In the case of anti-plane shearing along the z-axis, we have

$$\tau_{xz}(x, y, t) = \mu(D)\frac{\partial}{\partial x}u_z(x, y, t), \tag{1a}$$

$$\tau_{yz}(x, y, t) = \mu(D)\frac{\partial}{\partial y}u_z(x, y, t), \tag{1b}$$

$$\nabla_{xy}^2 u_z = \frac{\rho}{\mu(D)} \frac{\partial^2 u_z}{\partial t^2}, \tag{2}$$

where $\mu = Q/P$, polynomials $P(D)$ and $Q(D)$ are differential operators containing $D \equiv \partial/\partial t$, $\nabla_{xy}^2 = [(\partial^2/\partial x^2) + (\partial^2/\partial y^2)]$ is the Laplace operator, and ρ is the mass density of the material.

In the case of radial shearing inside the (x, y) or, in polar coordinates, (r, θ) plane, and when the Poisson's ratio is constant, we have

$$u_r(r, z, t) = \frac{\partial \phi}{\partial r} - \frac{\partial \psi}{\partial z}, \tag{3a}$$

$$u_z(r, z, t) = \frac{\partial \phi}{\partial z} + \frac{\partial \psi}{\partial r} + \frac{\psi}{r}, \tag{3b}$$

$$\sigma_r(r, z, t) = 2\mu(D) \frac{\partial}{\partial r}\left(\frac{\partial \phi}{\partial r} - \frac{\partial \psi}{\partial z}\right) + \lambda(D)\nabla_{rz}^2 \phi, \tag{4a}$$

$$\sigma_\theta(r, z, t) = 2\mu(D) \frac{1}{\partial r}\left(\frac{\partial \phi}{\partial r} - \frac{\partial \psi}{\partial z}\right) + \lambda(D)\nabla_{rz}^2 \phi, \tag{4b}$$

$$\sigma_z(r, z, t) = 2\mu(D) \frac{\partial}{\partial z}\left(\frac{\partial \phi}{\partial z} + \frac{\partial \psi}{\partial r} + \frac{\psi}{r}\right) + \lambda(D)\nabla_{rz}^2 \phi, \tag{4c}$$

$$\tau_{rz}(r, z, t) = \mu(D)\left[\frac{\partial}{\partial z}\left(2\frac{\partial \phi}{\partial r} - \frac{\partial \psi}{\partial z}\right) + \frac{\partial}{\partial r}\left(\frac{\partial \psi}{\partial r} + \frac{\psi}{r}\right)\right], \tag{4d}$$

where $\lambda = R/P$, $R(D)$ is again a differential operator, $\nabla_{rz}^2 = [(\partial^2/\partial r^2) + (1/r)(\partial/\partial r) + (\partial^2/\partial z^2)]$, and the *displacement potentials* $\phi(r, z, t)$, $\psi(r, z, t)$ satisfy wave equations containing differential operators as coefficients

$$\nabla_{rz}^2 \phi = \frac{1}{[c_1(D)]^2} \frac{\partial^2 \phi}{\partial t^2}, \quad c_1 = \left[\frac{\lambda(D) + 2\mu(D)}{\rho}\right]^{1/2}, \tag{5a}$$

$$\nabla_{rz}^2 \psi - \frac{\psi}{r^2} = \frac{1}{[c_2(D)]^2} \frac{\partial^2 \psi}{\partial t^2}, \quad c_2 = \left[\frac{\mu(D)}{\rho}\right]^{1/2}. \tag{5b}$$

The c_1 and c_2 operators degenerate in the pure-elastic case into the longitudinal and shear *wave velocities*.

In the case of torsional loading about the z-axis, we have

$$\tau_{r\theta} = \mu(D)\left(\frac{\partial u_\theta}{\partial r} - \frac{u_\theta}{r}\right), \tag{6a}$$

$$\tau_{\theta z} = \mu(D) \frac{\partial u_\theta}{\partial z}, \tag{6b}$$

$$\frac{\partial^2 u_\theta}{\partial r^2} + \frac{1}{r}\frac{\partial u_\theta}{\partial r} - \frac{u_\theta}{r^2} + \frac{\partial^2 u_\theta}{\partial z^2} = \frac{\rho}{\mu(D)} \frac{\partial^2 u_\theta}{\partial t^2}. \tag{7}$$

When the special case of the *standard linear solid* is considered, along with the additional assumption that the viscoelastic behaviour in bulk and in shear is identical, the Lamé operators take the form

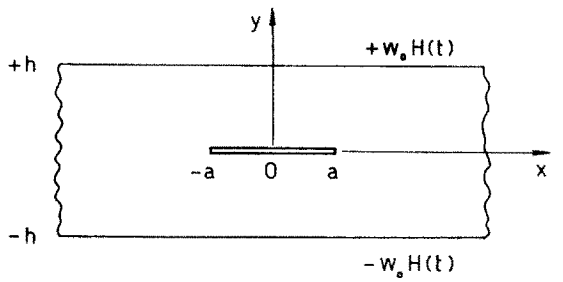

Fig. 1. Semi-infinite viscoelastic strip containing a stationary crack under anti-plane shear impact displacements.

$$\mu(D) = \mu_\infty \frac{\dfrac{\partial}{\partial t} + \dfrac{1}{\tau}}{\dfrac{\partial}{\partial t} + \dfrac{1+f}{\tau}}, \quad \lambda(D) = \frac{2\nu}{1-2\nu}\mu(D), \tag{8}$$

where $f = [(\mu_\infty/\mu_0) - 1]$ is a measure of the difference between the short-time, μ_∞, and the long-time, μ_0, shear moduli and $[\tau/(1+f)]$ is the relaxation time. The Poisson's ratio, ν is assumed to remain constant through the deformation process and this simplifies the analysis a little.

With eqns (1)–(8), the basic relations describing the material response were completed and we now direct attention to the boundary conditions of the specific problems considered here.

In the first case, we consider a body in the form of an infinite strip of height $2h$ containing a central crack of length $2a$, see Fig. 1. The loading consists of impact displacements $u_z(x, \pm h, t) = \pm w_0 H(t)$ applied along the lateral strip faces. However, solving the following auxiliary problem suffices for our purpose, i.e. determining the SIF

$$u_z(x, +h, t) = 0 \qquad \text{for } -\infty < x < \infty, \tag{9a}$$

$$u_z(x, 0, t) = 0 \qquad \text{for } |x| > a, \tag{9b}$$

$$\tau_{yz}(x, 0^+, t) = -\mu(D)\frac{w_0}{h}H(t) \quad \text{for } |x| < a. \tag{9c}$$

Quiescent initial conditions, i.e. $u_z = \dot{u}_z = 0$ for $t \leqslant 0$ are relevant to the problem.

In the second case, a state of pure radial shear is obtained if the transient wave incident to the penny-shaped crack produces only radial displacement $u_r(r, z, t)$ in the solid, whereas $u_\theta = u_z = 0$. This state can be achieved when the only stress component, $\tau_{rz}(r, z, t)$ contains a Heaviside step function of time. As in the previous case, the following auxiliary BVP suffices for determining the transient SIF (see Fig. 2)

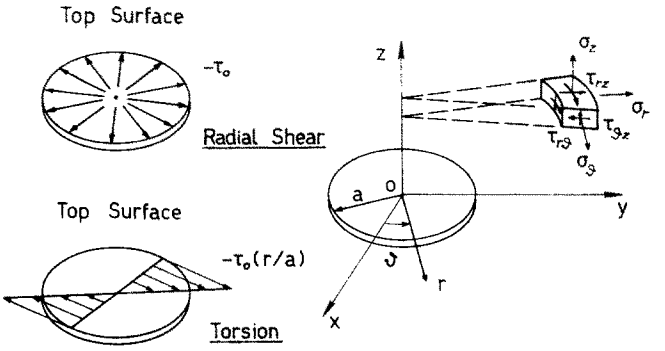

Fig. 2. Penny-shaped cracks in a viscoelastic body of infinite extent under radial-shear and torsional impact. The stress components in cylindrical polar coordinates are also indicated.

$$\tau_{rz}(r,0^+,t) = -\tau_0 H(t) \quad \text{for } r < a, \tag{10a}$$

$$\sigma_z(r,0^+,t) = 0 \quad \text{for } 0 < r < \infty, \tag{10b}$$

$$u_r(r,0^+,t) = 0 \quad \text{for } r > a, \tag{10c}$$

$$u_r(r,z,t) = 0 \quad \text{for } (r^2+z^2)^{1/2} \to \infty. \tag{10d}$$

Quiescent initial conditions are also assumed.

In the third case, the crack of diameter $2a$ is acted upon by impact torsional tractions of amplitude τ_0 (see Fig. 2). The boundary conditions are written as

$$\tau_{\theta z}(r, z = 0^+, t) = -\tau_0\left(\frac{r}{a}\right)H(t) \quad \text{for } r < a, \tag{11a}$$

$$u_\theta(r, z = 0^+, t) = 0 \quad \text{for } r > a, \tag{11b}$$

$$u_\theta = 0 \quad \text{for } (r^2+z^2)^{1/2} \to \infty. \tag{11c}$$

The object of the present work is to determine viscoelastodynamic SIFs for the problems defined by (9), (10) and (11).

ANALYTICAL FORM OF SOLUTION

First, the following definitions of integral transforms are presented

$$f^*(p) = \int_0^\infty f(t)\,\mathrm{e}^{-pt}\,\mathrm{d}t, \quad f(t) = (2\pi\mathrm{i})^{-1}\int_{\mathrm{Br}} f^*(p)\,\mathrm{e}^{pt}\,\mathrm{d}p, \tag{12}$$

$$\bar{f}^*_{\mathrm{FC}}(s, y, p) = \int_0^\infty f^*(x, y, p)\cos(sx)\,\mathrm{d}x, \tag{13a}$$

$$\bar{f}^*_{\mathrm{H0}}(s, z, p) = \int_0^\infty f^*(r, z, p) r J_0(rs)\,\mathrm{d}r, \tag{13b}$$

$$\bar{f}^*_{\mathrm{H1}}(s, z, p) = \int_0^\infty f^*(r, z, p) r J_1(rs)\,\mathrm{d}r. \tag{13c}$$

The Laplace transform is utilized in all problems to suppress time, whereas the Fourier cosine transform is utilized in the anti-plane shear problem and the zero-order and first-order Hankel transforms are utilized in the axisymmetric problems.

The analytical part of solutions can be obtained by applying the above integral transforms to the governing equations and the boundary conditions, and then constructing *dual integral equations* for the unknown intensity functions (which are directly related to SIFs in the time domain). In the Laplace-transform domain, the dual IEs can be implicitly solved through the method of Noble (1963) by reduction to a second-kind Fredholm IE, the kernel of which is given in terms of an integral involving both a semi-infinite interval and an oscillatory integrand.

The analytical solution for the anti-plane shear problem was given previously by Georgiadis (1987), whereas the respective *purely elastic* radial shear and torsion problems were treated by Sih and Chen (1977). Therefore, for the latter cases, by invoking the *correspondence principle* (Tao, 1963; Achenbach, 1973), we can obtain a formal solution in the Laplace-transform domain. However, this is not of too much help from the numerical point of view, since the Laplace transformed *intensity* functions, $F^*(1,p)$, $G^*(1,p)$ and $H^*(1,p)$ below, depend already upon the material constants.

Under the following definition of the dynamic SIFs

$$k_{AS}(t) = \lim_{x \to +a} [[2(x-a)]^{1/2} \cdot \tau_{yz}(x, 0, t)], \tag{14a}$$

$$k_{RS}(t) = \lim_{r \to +a} [[2(r-a)]^{1/2} \cdot \tau_{rz}(r, 0, t)], \tag{14b}$$

$$k_{T}(t) = \lim_{r \to +a} [[2(r-a)]^{1/2} \cdot \tau_{\theta z}(r, 0, t)], \tag{14c}$$

for the anti-plane shear (AS), radial shear (RS) and torsion (T) problem, respectively, the analytical forms of solutions were found to be

$$k_{AS}(t) = \frac{w_0 a^{1/2}}{h} \frac{1}{2\pi i} \int_{Br} \mu^*(p) \frac{F^*(1, p)}{p} e^{pt} \, dp, \tag{15a}$$

$$k_{RS}(t) = \frac{\tau_0 a^{1/2}}{2} \frac{1}{2\pi i} \int_{Br} \frac{G^*(1, p)}{p} e^{pt} \, dp, \tag{15b}$$

$$k_{T}(t) = \frac{4\tau_0 a^{1/2}}{3\pi} \frac{1}{2\pi i} \int_{Br} \frac{H^*(1, p)}{p} e^{pt} \, dp, \tag{15c}$$

where the intensity functions result in the solution of the Fredholm IEs

$$F^*(\xi, p) + \int_0^1 K_{AS}(\xi, \eta, p) F^*(\eta, p) \, d\eta = \xi^{1/2}, \tag{16a}$$

$$G^*(\xi, p) + \int_0^1 K_{RS}(\xi, \eta, p) G^*(\eta, p) \, d\eta = \xi, \tag{16b}$$

$$H^*(\xi, p) + \int_0^1 K_{T}(\xi, \eta, p) H^*(\eta, p) \, d\eta = \xi^2. \tag{16c}$$

The kernels in (16) have the following forms

$$K_{AS} = (\xi\eta)^{1/2} \int_0^\infty [\gamma_2 \cdot \coth(\gamma_2 h) - s] \cdot J_0(s\xi) \cdot J_0(s\eta) \, ds, \tag{17a}$$

$$K_{RS} = (\xi\eta)^{1/2} \int_0^\infty s \cdot \left[\frac{\gamma_1}{\gamma_2} \cdot B\left(\frac{s}{\alpha}, p\right) - 1 \right] \cdot J_{3/2}(s\xi) \cdot J_{3/2}(s\eta) \, ds, \tag{17b}$$

$$K_{T} = (\xi\eta)^{1/2} \int_0^\infty (\gamma_2 - s) \cdot J_{3/2}(s\xi) \cdot J_{3/2}(s\eta) \, ds, \tag{17c}$$

where $J_0(\cdot)$, $J_{3/2}(\zeta) \equiv (2/\pi\zeta)^{1/2} [\sin(\zeta)/\zeta - \cos(\zeta)]$ are first-kind Bessel functions, and

$$B(s, p) = \frac{1}{2s\gamma_1(1-\kappa^2)} [[2s^2 + (p/c_2^*)^2]^2 - 4s^2\gamma_1\gamma_2] \left(\frac{c_2^*}{p}\right)^2, \tag{18}$$

where $\kappa = (c_2^*/c_1^*)^{1/2}$ and the longitudinal and shear-wave "speeds" are *complex* functions of the Laplace-transform variable p

$$c_1^*(p) = \left(\frac{\lambda^* + 2\mu^*}{\rho}\right)^{1/2}, \quad c_2^*(p) = \left(\frac{\mu^*}{\rho}\right)^{1/2}, \tag{19}$$

whereas the functions $\gamma_j (j = 1, 2)$ in (17) are given by

$$\gamma_j = \left[s^2 + \left(\frac{p}{c_j^*(p)} \right)^2 \right]^{1/2}. \tag{20}$$

Note that in (19) the Riemann sheet is chosen so that $c_j^*(p) > 0$ on the positive real axis, and any required branch cuts are taken to the left. Moreover, to define $\gamma_j(p, s)$ as analytic functions, the p-plane must be cut appropriately. In view of the *finiteness condition*, the branches of $\gamma_j(p, s)$ should be defined so that $\mathrm{Re}\,[\gamma_j(p, s)] > 0$. Since also, we are aiming at a Laplace-transform inversion of the solution by means of a Bromwich-path integral, an inspection should be made about possible *poles* and *branch cuts* of the integrands in the $\mathrm{Re}\,(p) > 0$ half-plane. Obviously, whether or not the p-plane can be cut appropriately will depend upon the forms of the viscoelastic Lamé functions $\lambda^*(p)$ and $\mu^*(p)$ of the *particular* material.

The latter inspection was performed here for the standard linear solid, see (8), where the complex Lamé functions are given as

$$\mu^*(p) = \mu_\infty \frac{p + \dfrac{1}{\tau}}{p + \dfrac{1+f}{\tau}}, \quad \lambda^*(p) = \frac{2\nu}{1-2\nu}\mu^*(p). \tag{21}$$

The symbolic-manipulations program DERIVE was utilized for all numerical values of the standard-linear-solid constants considered for deriving the results in the last section of the paper. In all cases, we found that the branch cuts for $\gamma_j(p, s)$ were extending parallel to the negative $\mathrm{Re}\,(p)$-axis emanating from branch points in the $\mathrm{Re}\,(p) < 0$ half-plane. Thus, the integrands in (15) are always *analytic* functions in $\mathrm{Re}\,(p) > 0$ and consequently the integrals in (15) are amenable to Laplace-transform inversion by means of a Bromwich-path integral.

LAPLACE TRANSFORM INVERSION

The inversion of the Laplace transform in (15) was carried out numerically by following the DAC technique (Dubner and Abate, 1968; Crump, 1976). In this section, this technique will be briefly described.

One may start from eqn (12) and notice the following alternative form of the original function $f(t)$

$$f(t) = (e^{ct}/\pi) \int_0^\infty [\mathrm{Re}\, f^*(c+iu) \cdot \cos(ut) - \mathrm{Im}\, f^*(c+iu) \cdot \sin(ut)]\, du, \tag{22}$$

where $p = c+iu$. If the *trapezoidal* rule for integrals over semi-infinite intervals is applied to eqn (22), then the resulting approximate expression for $f(t)$ is a Fourier series (Davis and Rabinowitz, 1984)

$$f(t) \cong (e^{ct}/T)\left[\frac{1}{2} f^*(c) + \sum_{k=1}^{\infty} [\mathrm{Re}\, f^*(c+ik\pi/T) \cdot \cos(k\pi t/T) - \mathrm{Im}\, f^*(c+ik\pi/T) \cdot \sin(k\pi t/T)] \right]. \tag{23}$$

Crump (1976) has presented a systematic analysis of errors in the above procedure, from which one can compute $f(t)$ to a predetermined accuracy. First, T is chosen so that $2T > t_{\max}$ and then c is computed by

$$c = q - (\ln(E'))/2T, \tag{24}$$

Table 1. Laplace-transform inversion results by the Miller/Guy and DAC techniques for a function with an exact original

	$f(t) = (t/2)\sin t, \quad f^*(p) = p/(p^2+1)^2$			
t	Miller/Guy $f(t)$ ($\beta = 1.50, \delta = 0.75$)	Miller/Guy $f(t)$ ($\beta = 1.00, \delta = 1.00$)	DAC $f(t)$	Exact $f(t)$
0.0	−0.0034	−0.0063	0.00002	0.00000
1.0	0.4210	0.4182	0.41986	0.42073
2.0	0.9045	0.9143	0.90899	0.90929
3.0	0.2008	0.2313	0.21168	0.21168
4.0	−1.5383	−1.5012	−1.51361	−1.51360
5.0	−2.3266	−2.0712	−2.39730	−2.39731
6.0	−0.7197	−2.0355	−0.83824	−0.83824
7.0	1.4041	−1.9608	2.29945	2.29945
8.0	2.9049	−1.9230	3.95743	3.95743

where q is a number slightly larger than max [Re (P) ; P is a pole of $f^*(p)$] and the relative error is to be no greater than E' (say $E' = 10^{-8}$). It is possible also to increase the rate of convergence of (23) and thus reduce the truncation error by using a suitable series transformation. Crump recommends the *epsilon algorithm* (Abramowitz and Stegun, 1972) which was also adopted in Georgiadis (1991) and in the present study.

As a demonstration of the efficacy of the DAC technique and its superiority over the Miller/Guy technique, the results in Table 1 are presented. A Laplace-transformed function with an *exact* inversion was chosen as $f^*(p) = p/(p^2+1)^2$, whereas $N = 19$ and $N = 30$ was taken in the Miller/Guy and DAC, respectively. It is seen from the Table the strong dependence of the Miller/Guy results upon the choice of the β and δ parameters and the inaccuracy of the latter technique. Note also that the DAC technique is essentially similar to the Durbin technique employed by Narayanan and Beskos (1982).

NUMERICAL PROCEDURE

First, the integral equations (16) have to be solved numerically. Since these equations contains complex functions, we have to separate real from imaginary parts in the following manner

$$F^*(\xi, p) = F_1^*(\xi, \mathrm{Re}\, p, \mathrm{Im}\, p) + \mathrm{i}F_2^*(\xi, \mathrm{Re}\, p, \mathrm{Im}\, p), \tag{25}$$

$$K_{\mathrm{AS}}(\xi, \eta, p) = K_{\mathrm{AS1}}(\xi, \eta, \mathrm{Re}\, p, \mathrm{Im}\, p) + \mathrm{i}K_{\mathrm{AS2}}(\xi, \eta, \mathrm{Re}\, p, \mathrm{Im}\, p). \tag{26}$$

Then, eqn (16a) is equivalent to the following *coupled* Fredholm integral equations

$$F_1^* + \int_0^1 (K_{\mathrm{AS1}} \cdot F_1^* - K_{\mathrm{AS2}} \cdot F_2^*)\, \mathrm{d}\eta = \xi^{1/2}, \tag{27a}$$

$$F_2^* + \int_0^1 (K_{\mathrm{AS2}} \cdot F_1^* + K_{\mathrm{AS1}} \cdot F_2^*)\, \mathrm{d}\eta = 0. \tag{27b}$$

Similar expressions are also obtained for the $G^*(\xi, p)$ and $H^*(\xi, p)$ intensity functions.

The above two-dimensional systems were solved for $F^*(\xi, \mathrm{Re}\, p, \mathrm{Im}\, p)$, $G^*(\xi, \mathrm{Re}\, p, \mathrm{Im}\, p)$ and $H^*(\xi, \mathrm{Re}\, p, \mathrm{Im}\, p)$ by using the Gauss quadrature in conjunction with *complex algebra* on the computer. Since $p = c + \mathrm{i}(k\pi/T)$ is a parameter in (27), these equations have to be solved a number of times equal to the number of terms considered in the Laplace transform inversion (23).

Since $\xi, \eta < 1$, the integral giving the kernels K_{AS}, K_{RS} and K_{T} in (17) is not highly oscillatory, the standard *Gauss rule* can be applied. The semi-infinite interval was normalized to $[-1, +1]$ by the Stieltjes transformation (Davis and Rabinowitz, 1984). The above

procedure was checked both by the *IMT rule* (which is convenient for integrands with end-point singularities) and the *Longman rule* (which is convenient for oscillatory integrals over infinite intervals) (Davis and Rabinowitz, 1984) and found to be competitive. Thus, we utilized the simple Gauss rule throughout the numerical procedure, and evaluated the kernels with respect to p. The $J_0(\cdot)$ Bessel function appearing in (17a) was approximated by convenient polynomial forms (Abramowitz and Stegun, 1972).

For instance, the discretized form of the system (27) is as follows

$$F_1^*(x_i,p)+\sum_{j=n/2+1}^{n} Q_j\left[(x_ix_j)^{1/2}\cdot\sum_{k=1}^{n} Q_k\cdot M_1(x_i,x_j,x_k,p)\right]\cdot F_1^*(x_j,p)-\sum_{j=n/2+1}^{n} Q_j\left[(x_ix_j)^{1/2}\cdot\sum_{k=1}^{n} Q_k\cdot M_2(x_i,x_j,x_k,p)\right]\cdot F_2^*(x_j,p)=x_i^{1/2}, \quad (28a)$$

$$F_2^*(x_i,p)+\sum_{j=n/2+1}^{n} Q_j\left[(x_ix_j)^{1/2}\cdot\sum_{k=1}^{n} Q_k\cdot M_2(x_i,x_j,x_k,p)\right]\cdot F_1^*(x_j,p)+\sum_{j=n/2+1}^{n} Q_j\left[(x_ix_j)^{1/2}\cdot\sum_{k=1}^{n} Q_k\cdot M_1(x_i,x_j,x_k,p)\right]\cdot F_2^*(x_j,p)=0, \quad (28b)$$

where $i=1,2,\ldots,n/2$, n is the number of Gauss-quadrature collocation points, Q_j and Q_k are the Gauss-quadrature weights, and x_i, x_j, x_k are the Gauss-quadrature collocation points. Moreover, the complex kernel function in (28) is given as follows [see equation (17a)]

$$M(x_i,x_j,x_k,p)=\left[\gamma_{k,p}\cdot\coth(\gamma_{k,p}h)-\frac{1+x_k}{1-x_k}\right]\cdot J_0\left(x_i\frac{1+x_k}{1-x_k}\right)\cdot J_0\left(x_j\frac{1+x_k}{1-x_k}\right)\cdot\frac{2}{(1-x_k)^2}, \quad (29)$$

$$M(x_i,x_j,x_k,p)=M_1(x_i,x_j,x_k,\operatorname{Re}p,\operatorname{Im}p)+iM_2(x_i,x_j,x_k,\operatorname{Re}p,\operatorname{Im}p), \quad (30)$$

where

$$\gamma_{k,p}=\left[\left(\frac{1+x_k}{1-x_k}\right)^2+(p/c_2^*)^2\right]^{1/2}. \quad (31)$$

After determining the complex intensity functions $F^*(1,p)$, $G^*(1,p)$ and $H^*(1,p)$, the next step is the numerical inversion of the Laplace transforms in (15). However, before applying the DAC technique, we normalize both the SIFs and the time in the following way

$$m_{AS}(t)=\frac{h}{\mu_\infty w_0\alpha^{1/2}}k_{AS}(t), \quad m_{RS}(t)=\frac{2}{\tau_0\alpha^{1/2}}k_{RS}(t),$$

$$m_T(t)=\frac{3\pi}{4\tau_0\alpha^{1/2}}k_T(t), \quad (32)$$

and

$$p=\frac{c_2^\infty}{\alpha}w, \quad t=\frac{\alpha}{c_2^\infty}T_d, \quad (33)$$

where $c_2^\infty=(\mu_\infty/\rho)^{1/2}$ is the *short-time* shear-wave velocity. Then, eqns (15) become

$$m_q(t) = \frac{1}{2\pi i}\int_{c-i\infty}^{c+i\infty} L_q(1, w)\, e^{wT_d}\, dw, \quad (q = AS, RS, T), \tag{34}$$

and further are approximated according to (23) as

$$m_q(t) = (e^{cT_d}/T)\left[\frac{1}{2}L_q(c) + \sum_{k=1}^{N} [\mathrm{Re}\, L_q(c+ik\pi/T)\cdot\cos(k\pi T_d/T) - \mathrm{Im}\, L_q(c+ik\pi/T)\cdot\sin(k\pi T_d/T)]\right], \tag{35}$$

where

$$L_{AS}(1, w) = \frac{\mu\left(\frac{c_2^2}{a}w\right) F^*\left(1, \frac{c_2^2}{a}w\right)}{\mu_\infty \qquad w}, \tag{36a}$$

$$L_{RS}(1, w) = \frac{G^*\left(1, \frac{c_2^2}{a}w\right)}{w}, \tag{36b}$$

$$L_T(1, w) = \frac{H^*\left(1, \frac{c_2^2}{a}w\right)}{w}, \tag{36c}$$

and N is the number of terms required to obtain convergence. In this study, 60–70 terms were usually enough to get very accurate results. Of course, the accelerating epsilon algorithm was also employed.

In our opinion, the only disadvantage of the above-described numerical procedure is the large computation time involved. This is mainly due to the fact that the system (27) has to be solved the same number of times as are required for the respective number of terms in the approximation of the Laplace-transform inversion.

RESULTS AND CONCLUDING REMARKS

Numerical results for the dynamic SIFs were obtained for a material with constant short-time modulus $\mu_\infty = 1268$ MN m^{-2}, Poisson's ratio $\nu = 0.345$ and density $\rho = 1200$ kg m^{-3}, and variable f, τ in each case. The latter groups of material constants were considered in order to examine the effect of the viscoelastic behaviour.

In all cases, relations (8) pertinent to the *standard linear solid* were employed, whereas the complex Lamé functions are given by eqns (21). Clearly, in view of (8), the *purely elastic* case can be recovered from this material model by letting either $f \to 0$ or $\tau \to \infty$. Note also that the numerical values of f and τ utilized for obtaining our results fall into the range found in impact experiments employing PMMA (Nunziato *et al.*, 1974) and other polymers (Kuhn and Engel, 1973).

We quote also, for future usage, the following alternative to (8) representation of the standard-linear-solid response, which is based on the concept of relaxation functions $G_j(t)$ $(j = 1, 2)$

$$G_1(t) = \frac{\mu_\infty}{1+f}\left[1 + f\cdot\exp\left(-\frac{1+f}{\tau}t\right)\right], \tag{37a}$$

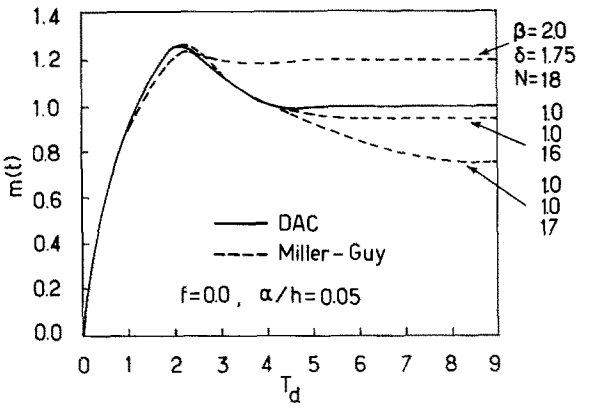

Fig. 3. Elastodynamic anti-plane shear SIF time history by the DAC and Miller/Guy inversion techniques. The static limit is $m(t = \infty) \cong 1$ in this case.

$$G_2(t) = \frac{2(1+\nu)}{1-2\nu} G_1(t). \tag{37b}$$

First, we present results for the anti-plane shear case.

Figure 3 shows the dynamic SIF time history in the case of a stationary crack under impact of an *elastic* ($f = 0.0$) plate of almost infinite extent ($a/h = 0.05$). The static limit for this problem is $m(t = \infty) \cong 1$, whereas a dynamic overshoot of about 25% occurs. For the purpose of comparison both the DAC and Miller/Guy techniques were utilized for this particular case. It can be clearly seen the strong dependence of the Miller/Guy results (Sih's procedure) on the choice of the parameters contained in these techniques. One can speak about a "non-uniqueness" of the results given by this method.

In Fig. 4, the influence of the strip height on the viscoelastodynamic SIF is presented. By reducing h, the SIF decreases. Furthermore, a comparison of the SIF time variation in Figs 3 (elastic case) and 4 (viscoelastic case) for $a/h = 0.05$ shows that the peak value for the SIF is lower in the viscoelastic problem but the difference between the maximum value and $m(T_d = 9)$ is greater in the viscoelastic problem. This means that in certain viscoelastic situations, there is the possibility of a much greater dynamic SIF overshoot in respect to the steady-state value than in the respective elastic case. Clearly, this is due to the continuous loss of energy in the viscoelastic body. The above SIF behaviour implies the necessity of performing a viscoelastodynamic analysis for cracked materials exhibiting a strong viscous effect, since a purely elastic analysis could give a rather conservative estimate of the dynamic SIF overshoot.

Finally, a comparison between Figs 4 ($f = 2.0$, $c_2^\infty \tau/h = 2.0$) and 5 ($f = 0.15$,

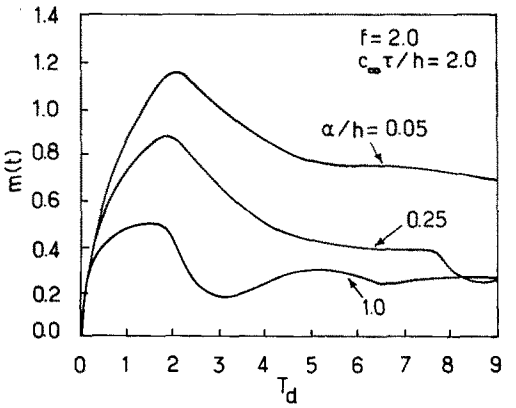

Fig. 4. Viscoelastodynamic anti-plane shear SIF time history for $\mu_\infty = 1268$ MN m^{-2}, $f = 2.0$, $c_2^\infty \tau/h = 2.0$ and variable strip height.

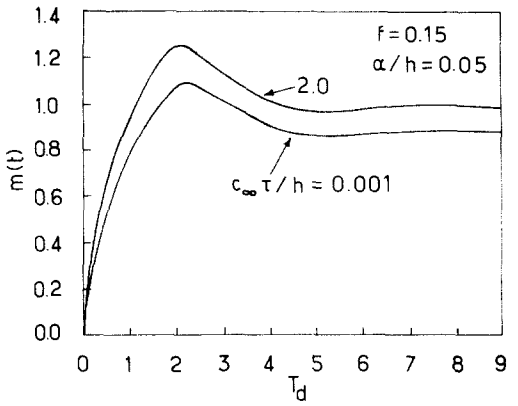

Fig. 5. Viscoelastodynamic anti-plane shear SIF time history for $\mu_\infty = 1268$ MN m^{-2}, $f = 0.15$, $a/h = 0.05$ and variable relaxation time.

$c_2^\infty \tau/h = 2.0$) indicates that by increasing the difference f between short- and long-time modulus, i.e. by increasing the viscous behaviour, the SIF decreases.

Next, we present results for the radial shear and torsion cases.

Figure 6 shows the dynamic SIF time history in the case of a stationary penny-shaped crack under radial-shear impact of an *elastic* ($f = 0.0$) body. The static limit for this problem is $m(t = \infty) = 1$ and so this may serve for checking the numerical results. Again, for the purpose of comparison, both the DAC and Miller/Guy techniques were utilized for this particular case. As previously, one may notice for this case also the radical dependence of the Miller/Guy results on the choice of the parameters contained in this technique. Figure 7 presents analogous results for the torsional impact case. Similar conclusions are also drawn.

In obtaining the results shown in Fig. 8, a small difference ($f = 0.15$) between the short- and long-time shear moduli was taken, whereas two different values of the relaxation time were considered ($c_2^\infty \tau/a = 100.0$ and 0.05), for the torsional case. We can observe from these results that the SIF–time curve closely resembles that of the elastic case, i.e. there is a dynamic overshoot at about $T_d = 1$ and then the SIF tends slowly to its steady-state value which is near $m = 1$. This is due to the almost identical values of μ_∞ and μ_0 and thus, even radical changes of the relaxation time produce no appreciable viscous effect.

However, strong viscous effects are observed in the results of Figs 9, 10 and 11, 12, where *medium* and *large* f was considered, respectively, for both the torsional and radial-shear states.

To obtain the SIF–time curves in Figs 9 and 10, $f = 2.0$ was taken, whereas the relaxation time was variable from large to small values. In the first case, $c_2^\infty \tau/a = 100.0$, the SIF time variation resembles the "elastic" one. In the second case, $c_2^\infty \tau/a = 2.0$, the viscous

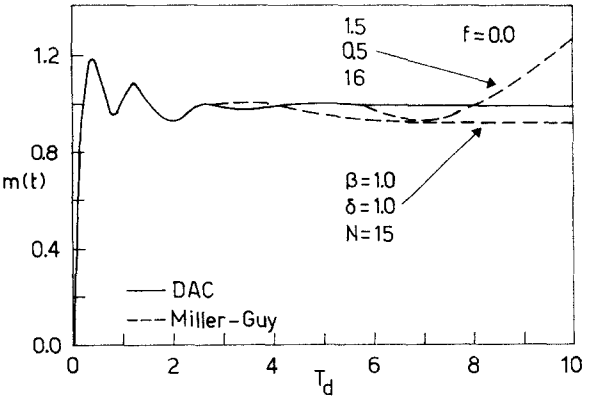

Fig. 6. Elastodynamic radial-shear SIF time history by the DAC and Miller/Guy inversion techniques. The static limit is $m(t = \infty) = 1$ in this case.

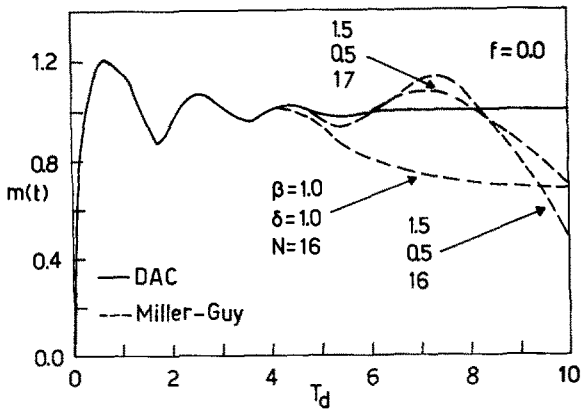

Fig. 7. Elastodynamic torsional SIF time history by the DAC and Miller/Guy inversion techniques. The static limit is $m(t = \infty) = 1$ in this case.

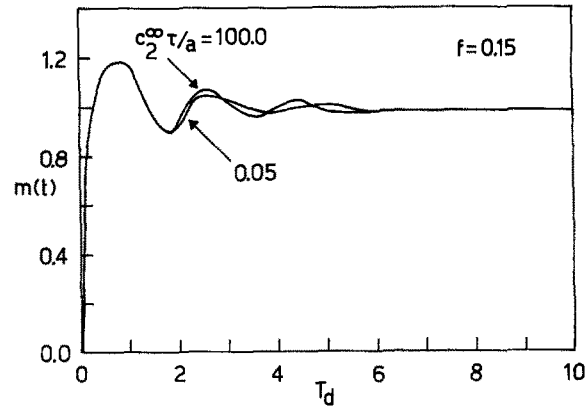

Fig. 8. Viscoelastodynamic torsional SIF time history for $\mu_\infty = 1268$ MN m^{-2}, $f = 0.15$ and variable relaxation time.

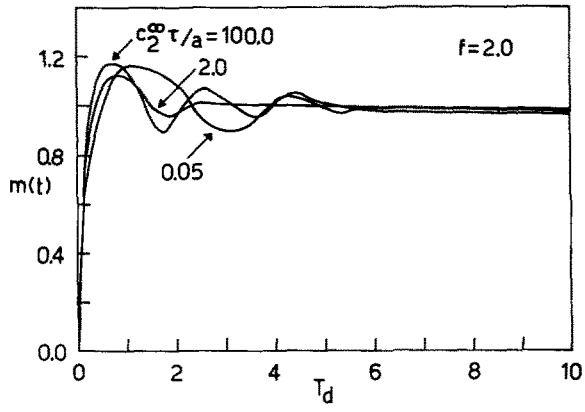

Fig. 9. Viscoelastodynamic torsional SIF time history for $\mu_\infty = 1268$ MN m^{-2}, $f = 2.0$ and variable relaxation time.

effect was pronounced since a very weak dynamic overshoot occurs. In the third case, $c_2^\infty \tau/a = 0.05$, one would expect perhaps a more viscous impact response and possible *no* dynamic overshoot in the SIF values because of the abrupt decrease of the relaxation functions in respect to time. However, an appreciable dynamic overshoot occurs but it is somewhat *delayed*. A similar observation can also be made in Figs 11 and 12.

This "unexpected" behaviour can be explained in view of Fig. 13, where the effect of large, medium and small relaxation time is shown upon the relaxation function. When the

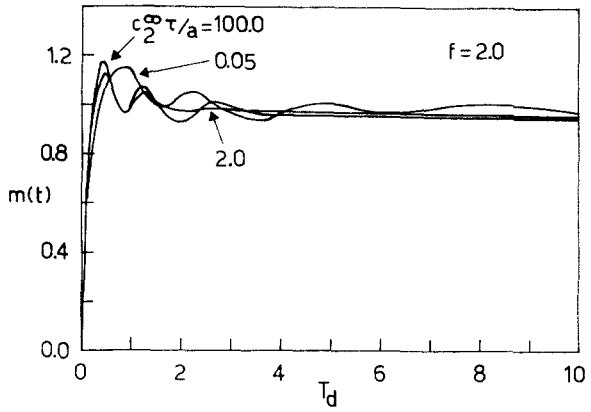

Fig. 10. Viscoelastodynamic radial-shear SIF time history for $\mu_\infty = 1268$ MN m^{-2}, $f = 2.0$ and variable relaxation time.

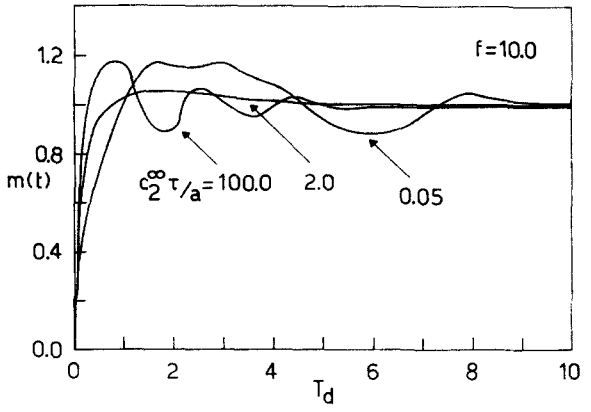

Fig. 11. Viscoelastodynamic torsional SIF time history for $\mu_\infty = 1268$ MN m^{-2}, $f = 10.0$ and variable relaxation time.

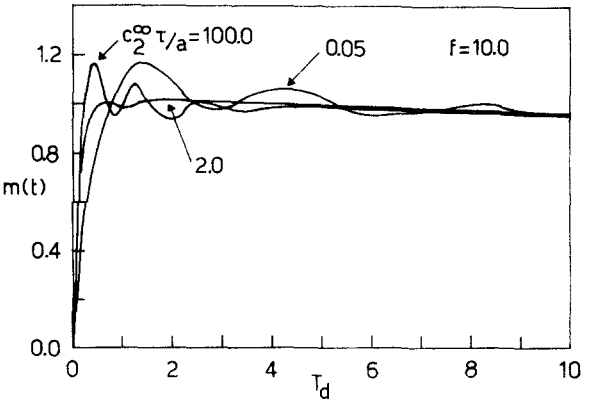

Fig. 12. Viscoelastodynamic radial-shear SIF time history for $\mu_\infty = 1268$ MN m^{-2}, $f = 10.0$ and variable relaxation time.

values $G(0)$ and $G(\infty)$ are fixed, in ranges where the $G(t)$ curve is almost flat and slowly decreasing, one should expect to observe *instantaneously*, an almost elastic material response, whereas in ranges of continuously varying $G(t)$ the viscous effect is more pronounced.

The delayed SIF dynamic overshoot for small τ is due to this *delayed elasticity* of the material model. The latter phenomenon is more vivid in Figs 11 and 12 for $f = 10.0$ and

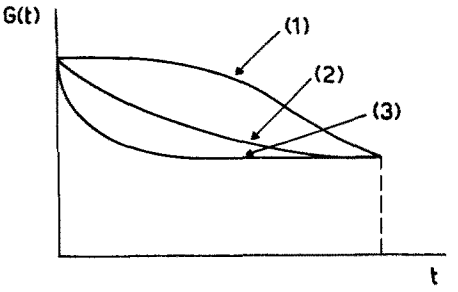

Fig. 13. Dependence of the relaxation function $G(t)$ on the relaxation time $[\tau/(1+f)]$ for the standard linear solid. Curve (1): large τ (pronounced elastic behaviour), Curve (2): medium τ, Curve (3): small τ (pronounced viscous behaviour).

$c_2^\infty \tau/a = 0.05$. Since the flat $-G(t)$ interval occurs after a longer time than in the case $f = 2.0$, the dynamic overshoot time-interval is observed now to be even more delayed.

Focusing our attention again on the results presented in Figs 11 and 12, we observe that a still appreciable dynamic overshoot occurs for very large relaxation time ($c_2^\infty \tau/a = 100.0$) but the steady-state limit is now more distant from the purely elastic one. For medium relaxation time ($c_2^\infty \tau/a = 2.0$) no SIF overshoot occurs.

In summarizing our numerical study, the following conclusions are quoted:

(1) When f is *small*, even radical changes of the relaxation time produce *no appreciable* viscous effect. *Strong* viscous effects are observed, when *medium* and *large* f is considered.

(2) When the values $G(t = 0)$ and $G(t = \infty)$ are fixed, in ranges where the $G(t)$ curve is almost *flat* and *slowly decreasing*, one should expect to observe instantaneously, an *almost elastic* material response (in respect to the overshoot of SIF), whereas in ranges of *continuously varying* $G(t)$ the *viscous* effect is more pronounced.

(3) Performing a viscoelastodynamic analysis for cracked materials is useful, since *unexpected* dynamic SIF overshoots may occur.

(4) A *pure elastic* analysis based on the steady-state viscoelastic material response may underestimate the SIF values.

REFERENCES

Abramowitz, M. and Stegun, I. (1972). *Handbook of Mathematical Functions*. Dover, NY.

Achenbach, J. D. (1971). In *Mechanics Today* (Edited by S. Nemat-Nasser), Vol. 1, pp. 1–57. Pergamon Press, London.

Achenbach, J. D. (1973). *Wave Propagation in Elastic Solids*. North-Holland, NY.

Achenbach, J. D. and Brock, L. M. (1973). In *Dynamic Crack Propagation* (Edited by G. C. Sih), pp. 529–541. Noordhoff, Leyden.

Atkinson, C. and List, R. D. (1972). A moving crack problem in a viscoelastic solid. *Int. J. Engng Sci.* **10,** 309–322.

Atkinson, C. and Popelar, C. H. (1979). Antiplane dynamic crack propagation in a viscoelastic strip. *J. Mech. Phys. Solids* **27,** 431–439.

Baker, B. R. (1962). Dynamic stresses created by a moving crack. *J. Appl. Mech.* **29,** 449–458.

Bellman, R., Kalaba, R. E. and Lockett, J. A. (1966). *Numerical Inversion of the Laplace Transform*. American Elsevier, NY.

Brock, L. M. (1975). Effects of secondary diffractions on the SIFs generated for a finite crack by a shear wave. *Int. J. Engng Sci.* **13,** 851–859.

Christensen, R. M. (1971). *Theory of Viscoelasticity*. Academic Press, NY.

Cost, T. L. (1964). Approximate Laplace transform inversions in viscoelastic stress analysis. *AIAA Jl* **2,** 2157–2166.

Crump, K. S. (1976). Numerical inversion of Laplace transforms using a Fourier Series approximation. *J. Assoc. Comp. Mach.* **23,** 89–96.

Datta, S. K. (1979). Diffraction of SH-wave by an edge crack. *J. Appl. Mech.* **46,** 101–106.

Davies, B. and Martin, B. (1979). Numerical inversion of the Laplace transform. A survey and comparison of methods. *J. Comp. Phys.* **33,** 1–32.

Davis, P. J. and Rabinowitz, P. (1984). *Methods of Numerical Integration*. Academic Press, NY.

Dubner, H. and Abate, J. (1968). Numerical inversion of Laplace transforms by relating them to the Finite Fourier Cosine transform. *J. Assoc. Comp. Mach.* **15,** 115–123.

Fung, Y. C. (1965). *Foundations of Solid Mechanics*. Prentice Hall, NJ.

Georgiadis, H. G. (1987). Finite length crack in a viscoelastic strip under impact—I. Theory. *Engng Fract. Mech.* **27,** 593–599.
Georgiadis, H. G. (1991). In *Dynamic Failure of Materials* (Edited by H. P. Rossmanith and A. J. Rosakis), pp. 296–308. Elsevier, London.
Georgiadis, H. G., Theocaris, P. S. and Mouskos, S. C. (1991). Plane impact of a cracked viscoelastic body. *Int. J. Engng Sci.* **29,** 171–177.
Karim, M. R. and Kundu, T. (1988). Transient surface response of layered isotropic and anisotropic half-spaces with interface cracks. SH-case. *Int. J. Fract.* **37,** 245–262.
Keogh, P. S. (1986). High-frequency scattering of a normally incident plane compressional wave by a penny-shaped crack. *Q. J. Mech. Appl. Math.* **39,** 535–566.
Kostrov, B. V. (1966). Unsteady propagation of longitudinal shear cracks. *J. Appl. Math. Mech. (PMM)* **30,** 1241–1248.
Krenk, S. and Schmidt, H. (1982). Elastic wave scattering by a circular crack. *Phil. Trans. R. Soc. London* **A308,** 167–198.
Kuhn, R. F. and Engel, P. A. (1973). Impact testing of viscoelastic materials. *Lett. Appl. Engng Sci.* **1,** 229–240.
Mal, A. K. (1970). Interaction of elastic waves with penny-shaped crack. *Int. J. Engng Sci.* **8,** 381–388.
Martin, P. A. and Wickham, G. R. (1983). Diffraction of elastic waves by a penny-shaped crack : analytical and numerical results. *Proc. R. Soc. London* **A390,** 91–129.
Miller, M. K. and Guy, W. T. (1966). Numerical inversion of the Laplace transform by use of Jacobi polynomials. *SIAM J. Numer. Anal.* **3,** 624–635.
Narayanan, G. V. and Beskos, D. E. (1982). Numerical operational methods for time-dependent linear problems. *Int. J. Numer. Meth. Engng* **18,** 1829–1854.
Noble, B. (1963). The solution of Bessel function dual integral equations by a multiplying-factor method. *Proc. Camb. Phil. Soc.* **59,** 351–362.
Nunziato, J. W., Walsh, E. K., Schuler, K. W. and Barker, L. M. (1974). In *Encyclopedia of Physics VIa/4 : Mechanics of Solids IV* (Edited by C. Truesdell), pp. 1–52. Springer, Berlin.
Papoulis, A. (1957). A new method of inversion of the Laplace transform. *Q. Appl. Math.* **14,** 405–414.
Popelar, C. H. and Kanninen, M. F. (1980). A dynamic viscoelastic analysis of crack propagation and crack arrest in a double cantilever beam test specimen. *ASTM STP* **711,** 5–23.
Sih, G. C. and Chen, E. P. (1977). In *Elastodynamic Crack Problems* (Edited by G. C. Sih). Noordhoff, The Netherlands.
Sih, G. C. and Chen, E. P. (1981). In *Cracks in Composite Materials* (Edited by G. C. Sih). Nijhoff, The Hague.
Tao, L. N. (1963). The associated elastic problems in dynamic visco-elasticity. *Q. Appl. Math.* **21,** 215–222.
Thau, S. A. and Lu, T. H. (1971). Transient stress intensity factors for a finite crack in an elastic solid caused by a dilatational wave. *Int. J. Solids Structures* **7,** 731–750.
Willis, J. R. (1967). Crack propagation in viscoelastic media. *J. Mech. Phys. Solids* **15,** 229–240.